

A BIOPHYSICAL MODEL FOR SEEDLING ESTABLISHMENT IN MANGROVE FORESTS

R. Gijssman¹, E.M. Horstman¹, P.W.J.M. Willemsen^{1,2}, A. Swales³, and K.M. Wijnberg¹
¹Marine and Fluvial Systems, Faculty of Engineering Technology, University of Twente, Enschede, The Netherlands r.gijssman@utwente.nl.
²Ecosystems and Sediment Dynamics, Deltares, Delft, The Netherlands.
³National Institute of Water and Atmospheric Research, Hamilton, New Zealand.

Abstract

Mangrove seedling establishment is crucial to the long-term development of mangrove forests. This study incorporates a process-based approach for seedling establishment in a process-based hydrodynamic model. The biophysical model is used to simulate seedling establishment in the Firth of Thames estuary (New Zealand). The results are compared to a random seedling establishment approach that has been often-used in long-term mangrove forest development models. While small differences were observed in terms of the seaward extent of seedling establishment, larger differences were found for the patchiness and density of the establishing seedlings. The results of the process-based approach showed a more localized pattern of seedling establishment, in line with field observations in the Firth of Thames. This pattern was opposed to the more spatially uniform establishment patterns predicted with the random establishment approach. These differences reveal that the implemented seedling establishment approach may affect long-term mangrove forest development models. Moreover, the process-based approach is more easily setup and calibrated with physical parameters that can be measured in the field.

1. Introduction

Intertidal mangrove vegetation has the ability to attenuate waves, accumulate sediments and stabilize shorelines. As such, mangroves are increasingly being considered as nature-based solutions to reduce coastal flood risk. Utilization of mangroves to reduce flood risk does, however, require assessment of their continued ecosystem functioning, or persistence (Gijssman et al., 2021). Predicting mangrove ecosystem functioning is a complex task because the decadal dynamics of mangroves are highly non-linear and can be limited by threshold conditions on timescales as short as days. For instance, mangrove vegetation can rapidly change due to weather anomalies on the timescale of days to weeks, causing conditions that may abruptly lead to tree mortality (e.g. a tropical cyclone) or trigger seedling establishment (e.g. a calm weather period).

Despite the importance of these short-term dynamics, models to assess mangrove forest development on a decadal timescale do not yet include vegetation change forced by hydrodynamic variations on these short timescales. This omission is mainly caused by the great computational expense of models resolving short-term hydrodynamics on a fine spatial grid for periods of several decades. Instead, existing long-term mangrove forest development models have assumed seedling establishment (e.g. Van Maanen et al., 2015) and abrupt tree mortality (e.g. Grueters et al., 2014) to occur randomly in space and time.

This study investigates the establishment of mangrove seedlings by implementing a process-based seedling establishment approach into a process-based hydrodynamic model (Delft3D Flexible Mesh). The seedling establishment model is partly based on the Windows of Opportunity (WoO) theory, which links the establishment of seedlings to periods of limited hydrodynamic exposure (Balke et al., 2011). This new model was used to simulate seedling establishment dynamics in the Firth of Thames estuary, New Zealand. Model results are compared to a random seedling establishment approach. This paper describes the model set-up and presents important differences between a random and a process-based seedling establishment approach in mangrove development models.

2. Methodology

2.1. Study area

This study considers a mangrove forest in the Firth of Thames (FoT) estuary, New Zealand. The FoT mangrove forest is approximately 1 km wide, relatively alongshore uniform and consists of a single mangrove species (*Avicennia marina*). This temperate forest is located near the southern limit of mangroves globally and tree heights are limited to < 4 m primarily by climate. The FoT mangroves have been monitored intensively for more than a decade (e.g. Swales et al., 2019). Of particular interest are the shore-normal elevation- and vegetation transects measured in November 2016 (Horstman et al., 2018). The transects span the mildly sloping unvegetated mudflat, steeper-sloped forest fringe and mature forest platform (Figure 1). The elevation profile was measured with a RTK-GPS, while 13 vegetation plots of 5x5 m² were selected for the vegetation (Montgomery et al., 2018). In addition, pressure sensors with a sampling frequency of 0.2 Hz were deployed along the same transect spanning the unvegetated mudflat and mangrove fringe forest in January 2020 (monitoring ongoing; Figure 1). Further details on the study area are presented in Swales et al., (2019).

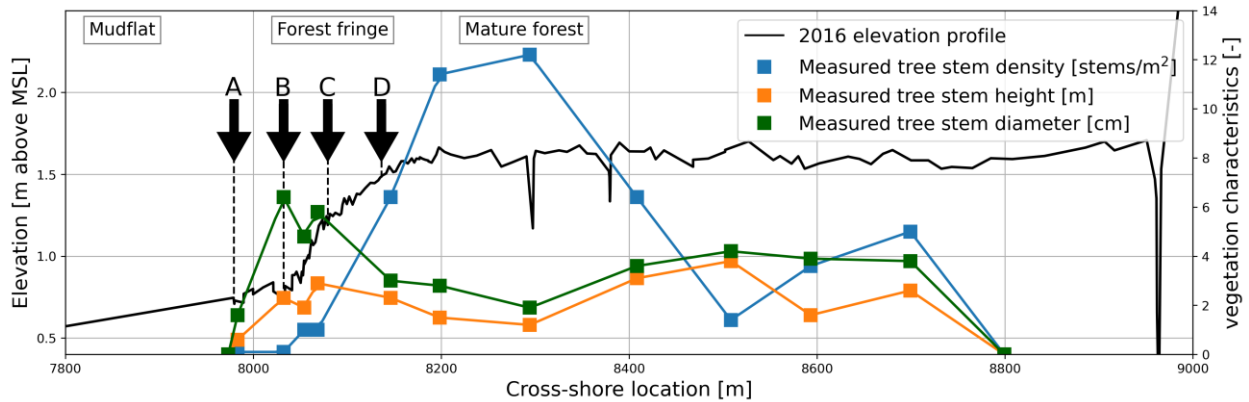


Figure 1: The elevation profile and mangrove stem density, height and diameter along a shore-normal transect in the Firth of Thames mangroves in 2016. Pressure sensors were installed at four measurement stations (indicated by arrows) in the forest fringe in 2020.

2.2. Hydrodynamic model description

The biophysical model solves hydrodynamic processes (e.g. tidal inundation and wind wave propagation) in a depth-averaged 2DH model of the study area (section 2.4). The hydrodynamic model is set-up in Delft3D-Flexible Mesh (DFM; Deltares, 2020a). DFM solves the depth-averaged continuity and momentum equations (Eq. 1 and Eq. 2, respectively). Wind and swell wave propagation and attenuation are solved with a wave energy balance (Eq. 3; Deltares, 2020b).

$$\frac{\delta h}{\delta t} + \frac{\delta hu}{\delta x} + \frac{\delta hv}{\delta y} = 0 \quad (1)$$

$$\frac{\delta u}{\delta t} + u \frac{\delta u}{\delta x} = -g \frac{\delta h}{\delta x} + v_v \frac{\delta^2 u}{\delta x^2} - g \cdot \frac{u|u|}{C^2 \cdot h} - \frac{\lambda}{2} u^2 \quad (2)$$

$$\frac{\delta N}{\delta t} + \frac{\delta c_x N}{\delta x} + \frac{\delta c_y N}{\delta y} + \frac{\delta c_\sigma N}{\delta \sigma} + \frac{\delta c_\theta N}{\delta \theta} = \frac{S}{\sigma} \quad (3)$$

In Eq. 1, h is the water level in [m], t is the time in [s], u is the flow velocity in x-direction in [$\text{m}\cdot\text{s}^{-1}$], x is the distance in x-direction (here defined as cross-shore) in [m], v is the flow velocity in y-direction in [$\text{m}\cdot\text{s}^{-1}$] and y is the distance in y-direction (here defined as longshore) in [m]. In Eq. 2, g is the gravitational acceleration of 9.81 [$\text{m}\cdot\text{s}^{-2}$], ν_v is the eddy viscosity which is set to 10 [$\text{m}^2\cdot\text{s}^{-1}$], C is the Chézy coefficient in [$\text{m}^{1/2}\cdot\text{s}^{-1}$] and λ is the vegetation resistance coefficient in [m^{-1}]. Lastly, in Eq. 3, N is the wave action density spectrum in [$\text{m}^2\cdot\text{Hz}^{-2}$], c_x is the propagation velocity in x-direction in [$\text{m}\cdot\text{s}^{-1}$], c_y is the propagation velocity in y-direction in [$\text{m}\cdot\text{s}^{-1}$], c_σ is the propagation velocity in σ -direction in [Hz^2] representing a shift in relative frequency due to depth- and current-induced variations, c_θ is the propagation velocity in θ -direction in [$\text{rad}\cdot\text{s}^{-1}$] representing refraction, σ is the relative frequency in [Hz] and θ the wave direction in [rad], S represents the effects of wave generation, dissipation and wave-wave interactions in [$\text{m}^2\cdot\text{Hz}^{-1}$].

The damping effect of the mangrove vegetation on tidal flows is incorporated in DFM by means of the Chézy coefficient and the vegetation resistance coefficient λ (Baptist et al., 2007; Eq. 4 and Eq. 5). The dissipating effect of mangrove vegetation on wave energy is incorporated in the sink term S of the wave-energy balance. The wave energy dissipation is implemented with a rate of energy dissipation ϵ_v in [$\text{N}\cdot\text{m}^{-1}\cdot\text{s}^{-1}$] (Mendez and Losada, 2004; Eq. 6).

$$C = C_b + \frac{\sqrt{g}}{\kappa} \ln\left(\frac{h}{h_v}\right) \sqrt{1 + \frac{C_D m d_v h_v C_b^2}{2g}} \quad (4)$$

$$\lambda = C_D \cdot m \cdot d_v \cdot \frac{h_v \cdot C_b^2}{h \cdot C^2} \quad (5)$$

$$\epsilon_v = \frac{\rho \cdot C_D \cdot m \cdot d_v}{2 \cdot \sqrt{\pi}} \cdot \left(\frac{g \cdot k}{2 \cdot \sigma}\right)^3 \cdot \frac{\sinh^3\left(k \cdot \frac{h_v}{h} \cdot h\right) + 3 \sinh\left(k \cdot \frac{h_v}{h} \cdot h\right)}{3k \sinh^3(k \cdot h)} \cdot H_{rms}^3 \quad (6)$$

In Eq. 4 and Eq. 5, C_b is the Chézy coefficient due to the bed roughness only in [$\text{m}^{1/2}\cdot\text{s}^{-1}$], κ is the dimensionless von Kármán constant, h_v is the height of the submerged part of the vegetation in [m], C_D is the dimensionless drag coefficient of the vegetation (see Table 1), m is the vegetation density in [$\text{stems}\cdot\text{m}^{-2}$] and d_v is the vegetation diameter in [m]. In the case of emergent vegetation ($h_v = h$; as typical for mangroves), Eq. 4 and Eq. 5 simplify to $C = C_b$ and $\lambda = C_D \cdot m \cdot d_v$, respectively. In Eq. 6, ρ is the water density in [$\text{kg}\cdot\text{m}^{-3}$], k is the wave number in [m^{-1}], σ is the wave frequency in [Hz], and H_{rms}^2 is the root-mean-squared wave height in [m].

This study implemented a Manning surface roughness coefficient n of 0.03 [$\text{s}\cdot\text{m}^{-1/3}$], following a model study of Horstman et al. (2015). The Manning surface roughness coefficient is related to the Chézy coefficient and the local water depth.

2.3. Mangrove seedling establishment model description

The seedling establishment process in the biophysical model consists of 3 stages: seedling delivery, root anchoring and seedling growth/survival. Seedling delivery is assumed to occur due to tidal inundation (Figure 2). Seedlings are delivered at the waterline where tidal inundation depths h_{inund} remain shallow (< 0.15 m). The delivery of seedlings is also limited to the fruiting season in which the mangrove trees produce seedlings. In the FoT estuary, the fruiting season takes place approximately from the 1st of November to the 1st of March. When seedling delivery occurs, the number of seedlings is set with a value for the seedling delivery density $n_{i,0}$ in [$\text{seedlings}\cdot\text{m}^{-2}$]. The location of the seedlings then varies randomly within the model grid cell.



Figure 2: Seedling propagule delivery on the mudflat in front of the Firth of Thames estuary mangroves. Picture taken by Erik Horstman in January 2020.

After seedling delivery, two sequential periods of no or limited hydrodynamic exposure are required as proposed in the Windows of Opportunity (WoO) theory (Balke et al., 2011). Firstly, seedling root anchoring requires an inundation-free period T_{WoO-1} of 3 days (Balke et al., 2015). Secondly, seedlings grow and the hydrodynamic threshold conditions the seedlings can cope with increase. In the biophysical model, the maximum bed shear stress for dislodgement τ_i in [$\text{N}\cdot\text{m}^{-2}$] is used to describe this threshold, following an initial growth study of *Avicennia marina* propagules in the FoT (Balke et al., 2015). The threshold bed shear stress is related to seedling root length, which is based on seedling age t_i in [days] (Eq. 11):

$$\tau_i = c_1 \cdot (c_2 \cdot t_i - c_3) - c_4 \quad (7)$$

In Eq. 11, c_1 [$\text{N}\cdot\text{m}^{-2}\cdot\text{cm}^{-1}$], c_2 [$\text{cm}\cdot\text{days}^{-1}$], c_3 [cm], c_4 [$\text{N}\cdot\text{m}^{-2}$] are calibration coefficients. Balke et al., (2015) estimated these coefficients to be $0.4135 \text{ N}\cdot\text{m}^{-2}\cdot\text{cm}^{-1}$, $0.3266 \text{ cm}\cdot\text{days}^{-1}$, 1.443 cm and $0.058 \text{ N}\cdot\text{m}^{-2}$, respectively, for *Avicennia marina* seedlings.

To compare the seedling establishment results with previous model approaches for decadal mangrove vegetation development, a random seedling establishment approach was setup next to the process-based approach. With the random establishment approach, the seedling delivery and root anchoring phases are not based considered to be based on hydrodynamic processes. Instead, a fixed total number of respectively 10, 100 and 200 seedlings establishes at every vegetation update and at random locations in the complete model domain. The threshold conditions for the survival of these seedlings then start to increase in the same way as in the process-based approach.

2.4. Model setup

The model was setup for the FoT estuary conditions. The model consists of a 100 m long alongshore uniform cross-section and a cross-shore extent of 8 km (Figure 3). An unstructured grid of 5050 cells was imposed with maximum grid cell sizes of 20x20 m² in the offshore areas and minimum grid cell sizes of 5x5 m² in the forest fringe area where the bed level gradient was greatest. The model bathymetry was based on the elevation profile of November 2016 (Figure 1), which was filtered with a median filter (windows of 5 m) after which perturbations with a maximum amplitude of 2 cm were randomly added to mimic local bed level variations.

The mangrove vegetation was implemented in the model based on the November 2016 field survey (Figure 1). The measured mangrove stem density and stem height were used to generate an individual-based tree model in three consecutive steps: (1) the stem height and stem density were linearly interpolated in the cross-shore direction (Figure 1), (2) the number of trees was determined for each 10 m cross-shore section of the model and these were randomly allocated within this section, (3) the stem height of each tree was randomly selected from a normal distribution, which was based on the mean and standard deviation in tree stem height reported in Montgomery et al., (2018). Lastly, tree stem density, stem height and stem diameter were averaged per grid cell (Figure 3).

The model simulation was performed for the period from 1st of November 2019 to 1st of June 2021 (19 months). Two fruiting seasons, i.e. from November to February, were included in which seedling delivery was possible. A water level boundary condition was imposed on the offshore model boundary, based on water level measurements at the nearby Tararu tidal station (Waikato Regional Council, Site Nr. 1033.1). A constant but small wave height (significant wave height H_s of 5 cm) was imposed on the offshore boundary to include small waves that were locally generated by wind. The hydrodynamic model timestep was limited to 30 s. Updates on the vegetation were performed at every low tide (average time interval of 12.4 hours), when the maximum inundation levels and bed shear stresses that occurred during the previous tide were extracted from the hydrodynamic model.

Table 1: Model parameter settings

<i>Parameter</i>	<i>Symb</i>	<i>Value</i>	<i>Unit</i>	<i>Reference</i>
	<i>ol</i>			
Manning coefficient	n	0.03	s·m ^{-1/3}	Horstman et al., (2015)
Grid cell drag coefficient	C_D	1	-	Nepf & Vivoni (2000)
Grid cell tree stem density	m	cell- averaged	trees·m ⁻²	Horstman et al., (2018)
Grid cell tree stem height	h_v	cell-averaged	m	Horstman et al., (2018)
Grid cell tree stem diameter	d_v	cell-averaged	m	Horstman et al., (2018)
Grid-cell bed level elevation	z_b	cell-averaged	m	Horstman et al., (2018)
Calibration coefficient	c_1	0.4135	N·m ⁻² ·cm ⁻¹	Balke et al., (2015)
Calibration coefficient	c_2	0.3266	cm·days ⁻¹	Balke et al., (2015)
Calibration coefficient	c_3	1.443	cm	Balke et al., (2015)
Calibration coefficient	c_4	0.058	N·m ⁻²	Balke et al., (2015)
Inundation depth for delivery	h_{inund}	0.15	m	
Seedling delivery density	$n_{i,0}$	0.03	seedlings·m ⁻²	
Inundation-free period	T_{woo-1}	3	days	Balke et al., (2015)

3. Results

3.1. Tidal inundations

The tidal inundation in the forest simulated by the model was compared with water depth measurements obtained with the pressure sensors (Figure 4). In general, the simulated water depths match the fluctuations of the measured tidal inundation on the timescale of days and months. Measured water depths started at approximately 25 cm due to the deployment height of the pressure sensors. At the three seaward measurement locations, the inundation peaks are slightly overestimated by the model (10-20 cm too high). These overestimations are likely the result of morphological changes that occurred between November 2016 (collection date of the bed level data) and January 2020 (the simulated tidal conditions). Since the bed elevation in the FoT mangrove forest fringe is known to be increasing (Swales et al., 2019), the bed level at pressure sensors A, B and C are likely underestimated. This underestimation leads to an overestimation of the water depths. Pressure sensor D is located in a less-active part of the profile. The slight underestimation of the water depth at sensor D could be caused by the discretization of the bed level elevation.

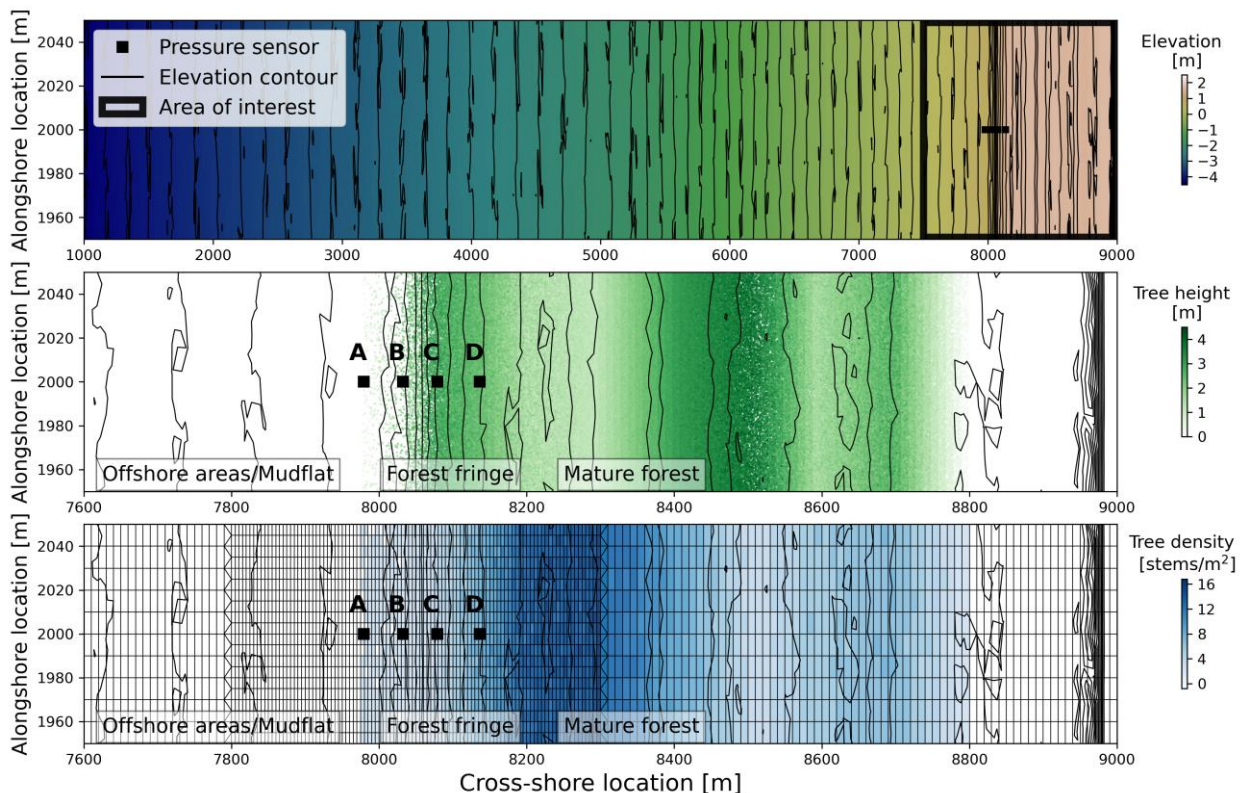


Figure 3: Bathymetry (top), location and stem height of the trees (centre, each individual tree is represented by a dot), and the numerical grid with the tree density averaged per grid cell (bottom). The locations of the pressure sensor in the forest fringe are indicated with black squares.

3.2. Seedling establishment and survival

The seedling establishment simulated with the process-based approach was analyzed and compared to the random establishment approaches (Figure 5). With the process-based approach, seedlings established at similar locations in the 2020 and 2021 fruiting seasons. The seedlings primarily established on the platform with an average elevation of 1.65 m above Mean Sea Level (MSL). The most seaward location of surviving seedlings was at an elevation of 1.41 m above MSL. In the simulations, it was observed that seedlings mostly established after spring tides, when the platform had been inundated and an inundation-free period followed. At these times, seedlings established down to an elevation of 1.16 m above MSL. However, these frontmost seedlings did (mostly) not survive during the following spring tide.

With the random establishment approach, bed level elevations where seedlings survived were similar to the process-based approach, mostly due to the many seedlings establishing on the platform with an elevation of 1.65 m above MSL. The seaward extent of the surviving seedlings was in the same order of magnitude but depended on the number of establishing seedlings. With 10 seedlings establishing per tide, the most seaward seedling was found at 1.43 m above MSL, while in the other two scenarios they were located at 1.18 m above MSL. This difference mainly occurred because favorable seedling establishment conditions were or were not captured by the random allocation of the seedling locations.

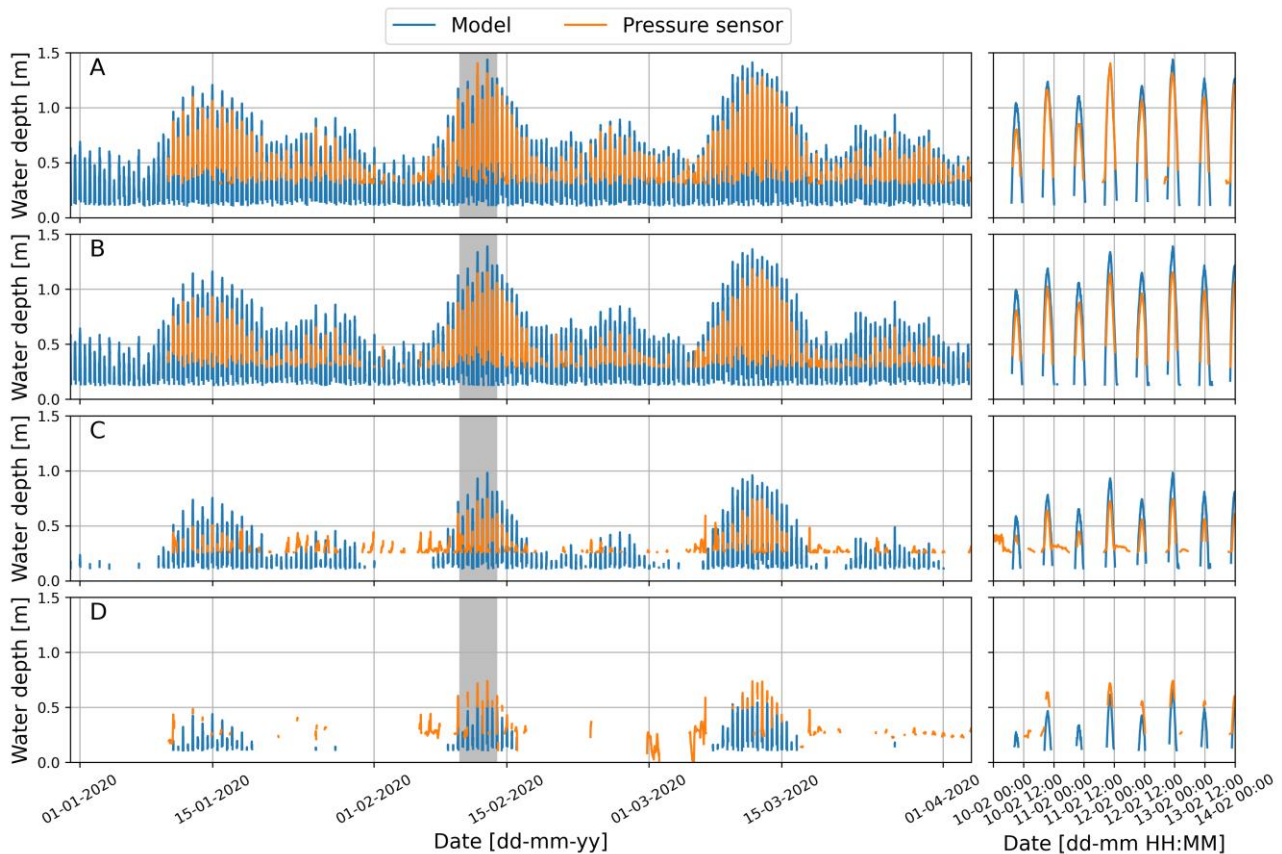


Figure 4: Comparison between monthly (left) and daily (right) variability in simulated and measured inundation depths at the four monitoring stations in the Firth of Thames.

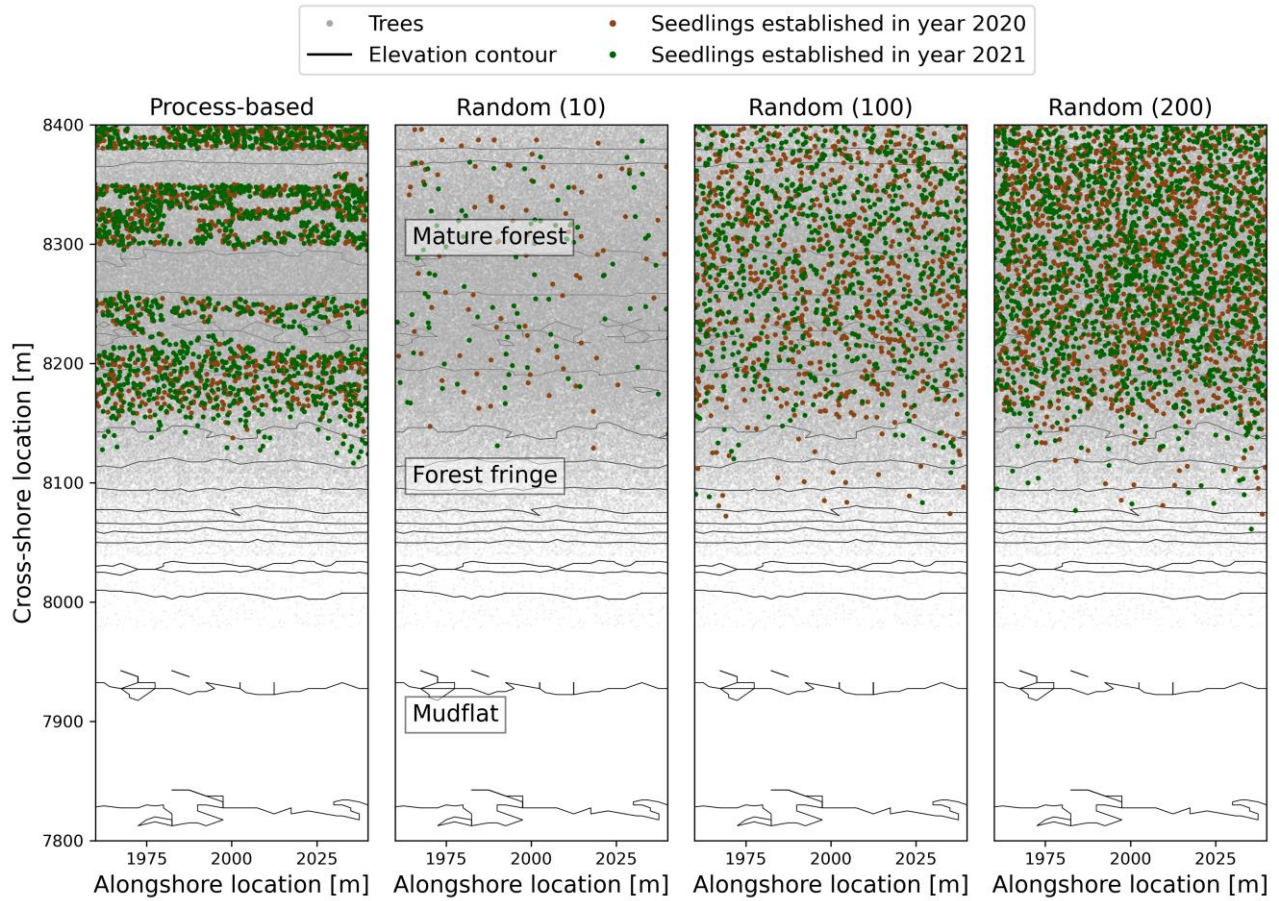


Figure 5: Comparison between process-based approach (left) and random establishment approaches with 10, 100 and 200 seedlings (right) at the end of the simulation time (June 2021).

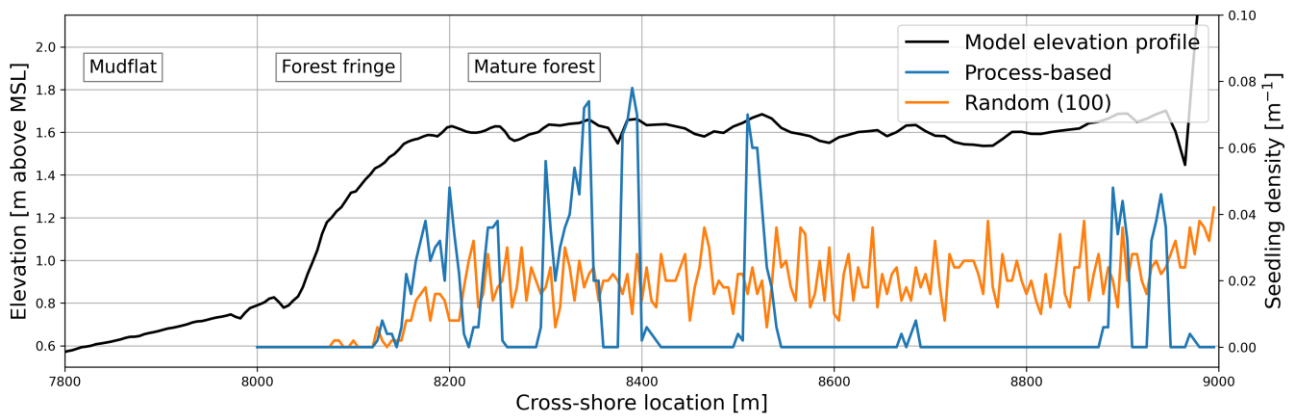


Figure 6: Comparison between seedling density with process-based approach and random establishment approach with 100 seedlings at the end of the simulation time (June 2021).

While the seaward extent of seedling establishment is similar between the two approaches, the patchiness and density of the seedlings varies largely between the process-based approach and the random establishment approach (Figure 5 and 6). The process-based model shows relatively large seedling densities at distinctive locations along the cross-shore profile. Particularly at the

upper extent of the forest fringe and at the slightly elevated areas of the platform, more seedlings were able to establish. This observation is in line with field observations of seedling colonization on top of mud bedforms (Swales et al., 2007). This contrasts to other areas of the coastal profile where no seedling establishment has taken place. The random establishment approach presents a gradually increasing density of seedlings across the forest fringe and a uniform spreading of seedlings across the forest platform, with a slight increase in the landward direction.

4. Discussion and Outlook

This study implemented a process-based seedling establishment approach in a process-based hydrodynamic model (Delft3D Flexible Mesh). The biophysical model was used simulate mangrove seedling establishment in the Firth of Thames (FoT) estuary in New Zealand. The process-based model results were compared to those with a random seedling establishment approach, that has been a widely used assumption in long-term mangrove development models.

Seedling establishment and growth in mangroves is largely affected by tidal inundation as well as disturbances due to wind waves and bed level changes. On longer timescales, ecological processes such as competition with existing vegetation can also play an important role (Berger and Hildebrandt, 2000). In the present model study, only the effects of tidal inundation and small wind waves were incorporated. Since the effects of events with larger wind waves, nor bed level changes, or tree competition were included, the model results can be regarded as a best-case scenario in terms of the long-term seedling survival probability.

In comparison to a random seedling establishment approach, the seaward extent of seedling establishment predicted with the process-based seedling establishment approach was found to be similar. The seaward extent was also in the same range as found in a previous study (Balke et al., 2015), where a slightly more seaward establishment of seedlings was predicted (down to elevations of 1.10m above MSL). The difference with previous findings may be caused by the consideration of different years. While this study only considered the establishment of seedlings in 2020 and 2021, the study of Balke et al. (2015) studied the years between 1993 and 2012. The presence of the El Niño – La Niña cycle at the field site can cause variable seedling establishment conditions between different years (Lovelock et al., 2010; Swales et al., 2015).

A larger difference between the process-based and random seedling establishment approach was found for the resulting mangrove seedling patchiness and density. While the process-based approach predicted a high seedling density at particular locations in the forest and forest fringe, the random establishment approach showed a more uniform seedling density throughout the forest. In this perspective, the process-based approach is more in line with long-term forest development in the FoT estuary. In the past, major seedling establishment events have been linked to rare hydrodynamic conditions. The effects of these rare events can still be observed in the forest characteristics, with a clear forest zonation of distinct tree height, diameter and density.

While the random establishment approach is highly sensitive to input parameters, particularly the number of establishing seedlings (Figure 5), the sensitivity of the process-based approach is based on physical parameters such as the inundation threshold for delivery, the required inundation-free period for seedling root anchoring and the seedling delivery density. These physical parameters allow for a more straightforward model setup and application to field sites, without the need for an extensive calibration of the random establishment parameters.

These new insights show the improved modelling capacity of the process-based mangrove seedling establishment model. In the future, this model will be extended with mangrove growth and survival dynamics in order to predict long-term mangrove forest development.

Acknowledgements

This study was part of the Mangrove-RESCUE project, funded by the Dutch Research Council (NWO Grant no. 15899), and was supported by the NIWA Strategic Science Investment Fund project (contract FWCE2104 Estuary Sediment Dynamics and Evolution).

References

- Balke, T., Bouma, T., Horstman, E., Webb, E., Erfteimeijer, P., and Herman, P. (2011). Windows of opportunity: Thresholds to mangrove seedling establishment on tidal flats. *Marine Ecology Progress Series*, 440: 1-9 <https://doi.org/10.3354/meps09364>
- Balke, T., Swales, A., Lovelock, C., Herman, P., and Bouman, T. (2015). Limits to seaward expansion of mangroves: Translating physical disturbance mechanisms into seedling survival gradients. *J. Exp. Marine Biol. Ecol.*, 467: 16-25 <https://doi.org/10.1016/j.jembe.2015.02.015>
- Baptist, M. J., Babovic, V., Uthurburu, J. R., Keijzer, M., Uittenbogaard, R. E., Mynett, A., et al. (2007). On inducing equations for vegetation resistance. *J. Hydraulic Res.* 45, 435–450 <https://doi.org/10.1080/00221686.2007.9521778>
- Berger, U., and Hildebrandt, H. (2000). A new approach to spatially explicit modelling of forest dynamics: Spacing, ageing and neighbourhood competition of mangrove trees. *Ecol. Model.* 132, 287302 [https://doi.org/10.1016/S0304-3800\(00\)00298-2](https://doi.org/10.1016/S0304-3800(00)00298-2)
- Deltares (2020a). *D-flow Flexible Mesh – User Manual*. Technical Report
- Deltares (2020b). *D-Waves – User Manual*. Technical Report
- Gijsman, R., Horstman, E., van der Wal, D., Friess, D., Swales, A., and Wijnberg, K. (2021). Nature-based engineering: A review on reducing coastal flood risk with mangroves. *Frontiers in Mar. Sci.* 8:702412 <https://doi.org/10.3389/fmars.2021.702412>
- Grueters, U., Seltman, T., Schmidt, H., Horn, H., Pranchai, A., Vovides, A.G., Peters, R., Vogt, J., Dahdouh-Guebas, F., and Berger, U., (2014), The mangrove forest dynamics model mesoFON. *Ecological Modelling*, 291: 28-41 <https://doi.org/10.1016/j.ecolmodel.2014.07.014>
- Horstman, E., Dohmen-Janssen, C., Bouma, T., and Hulscher, S. (2015). Tidal-scale flow routing and sedimentation in mangrove forests: combining field data and numerical modeling. *Geomorphology* 228: 244-262 <https://doi.org/10.1016/j.geomorph.2014.08.011>
- Horstman, E., Lundquist, C., Bryan, K., Bulmer, R., Mullarney, J., and Stokes, D. (2018). The dynamics of expanding mangroves in New Zealand, in *Threats to Mangrove Forests*. Eds C. Makowski and C. Finkle (Cham: Springer) https://doi.org/10.1007/978-3-319-73016-5_2
- Lovelock, C., Sorrell, B., Hancock, N., Hua, Q., and Swales, A. (2010). Mangrove forest and soil development on a rapidly accreting shore in New Zealand. *Ecosystems*. 13: 437-451 <https://doi.org/10.1007/s10021-010-9329-2>
- Mendez, F., and Losada, I. (2004). An empirical model to estimate the propagation of random breaking and nonbreaking waves over vegetation fields. *Coastal Eng.* 51: 103-118 <https://doi.org/10.1016/j.coastaleng.2003.11.003>
- Montgomery, J., Bryan, K., Horstman, E., and Mullarney, J. (2018). Attenuation of tides and surges by mangroves: contrasting case studies from New Zealand. *Water* 10:1119 <https://doi.org/10.3390/w10091119>
- Nepf, H.M. and Vivoni, E.R. (2000). Flow structure in depth-limited, vegetated flow. *J. Geophys. Res.*, 105(C12), 28547-28557 <https://doi.org/10.1029/2000JC900145>
- Swales, A., Bentley, S. J., Lovelock, C., and Bell, R. G. (2007). “Sediment processes and mangrove-habitat expansion on a rapidly-prograding muddy coast, New Zealand,” in *Coastal Sediments '07*, 1441–1454 [https://doi.org/10.1061/40926\(239\)111](https://doi.org/10.1061/40926(239)111)
- Swales, A., Bentley, S.J. and Lovelock, C.E. (2015). Mangrove-forest evolution in a sediment-rich estuarine system: opportunists or agents of geomorphic change? *Earth Surface Processes Landforms* 40, 1672-1687 <https://doi.org/10.1002/esp.3759>
- Swales, A., Reeve, G., Cahoon, D., and Lovelock, C. (2019). Landscape evolution of a fluvial sediment-rich avicennia marina mangrove forest: insights from seasonal and inter-annual surface elevation dynamics. *Ecosystems* 22: 1232-1255 <https://doi.org/10.1007/s10021-018-0330-5>
- Van Maanen, B., Coco, G., and Bryan, K. (2015). On the ecogeomorphological feedbacks that control tidal channel network evolution in a sandy mangrove setting. *Proc. R. Soc. A Math. Phys. Eng. Sci.* 471: 20150115 <https://doi.org/10.1098/rspa.2015.0115>